Konya Mühendislik Bilimleri Dergisi, c. 13, s. 2, 368-383, 2025
Konya Journal of Engineering Sciences, v. 13, n. 2, 368-383, 2025
ISSN: 2667-8055 (Electronic)
DOI: 10.36306/konjes.1587217

A COUPLED MCST-FEM INVESTIGATION OF SIZE-DEPENDENT BUCKLING OF PERFORATED NANOBEAMS ON WINKLER-PASTERNAK FOUNDATION

*** Uğur KAFKAS**

Kütahya Dumlupınar University, Vocational School of Technical Science, Construction Technology Department, Kütahya, TÜRKİYE
ugur.kafkas@dpu.edu.tr

Highlights

- Increasing Winkler and Pasternak foundation parameters enhances the critical buckling load
- Higher MCST length scale improves nanobeam stability, demonstrating nanoscale effects
- More holes reduce the critical buckling load by weakening structural stiffness
- Longer beams exhibit lower critical buckling loads even with a greater number of holes
- Nanoscale effects captured by MCST provide stability beyond classical beam theories

***Corresponding Author:** Uğur KAFKAS, ugur.kafkas@dpu.edu.tr

Konya Mühendislik Bilimleri Dergisi, c. 13, s. 2, 368-383, 2025
Konya Journal of Engineering Sciences, v. 13, n. 2, 368-383, 2025
ISSN: 2667-8055 (Electronic)
DOI: 10.36306/konjes.1587217

A COUPLED MCST-FEM INVESTIGATION OF SIZE-DEPENDENT BUCKLING OF PERFORATED NANOBEAMS ON WINKLER-PASTERNAK FOUNDATION

* Uğur KAFKAS

Kütahya Dumlupınar University, Vocational School of Technical Science, Construction Technology Department, Kütahya, TÜRKİYE
ugur.kafkas@dpu.edu.tr

(Received: 18.11.2024; Accepted in Revised Form: 26.02.2025)

ABSTRACT: The buckling behavior of perforated nanobeams on elastic foundations has become increasingly important, mainly due to their widespread use in nanostructures and nanotechnology systems. This study investigates the buckling behavior of perforated nanobeams resting on Winkler-Pasternak elastic foundations using Modified Couple Stress Theory (MCST) and the Finite Element Method (FEM). The analysis examines the effects of various parameters, including foundation elasticity, MCST internal length scale, perforation properties, and beam length, on critical buckling loads. Results indicate that increasing both Winkler and Pasternak foundation parameters enhances the critical buckling load, with the Pasternak parameter showing a more pronounced effect due to its incorporation of shear effects. The MCST internal length scale parameter significantly influences nano-beam stability, highlighting the importance of size effects at nanoscale dimensions. Higher filling ratios correlate directly with increased buckling resistance, while a greater number of holes reduces overall structural stiffness and decreases the critical buckling load. Beam length exhibits an inverse relationship with buckling strength; longer beams demonstrate lower critical buckling loads than shorter beams, regardless of the number of holes present.

Keywords: *Buckling Analysis, Finite Element Method, Modified Couple Stress Theory, Perforated Nanobeam, Winkler-Pasternak Foundation*

1. INTRODUCTION

Nanobeams are important nanostructures with many applications, including nanosystems, sensors, and micro/nano-electro-mechanical systems (MEMS-NEMS) [1]. The increasing use of perforated nanobeams, particularly when weight reduction or functional requirements necessitate structural modifications, has made it crucial to understand their mechanical behavior and study the effects of the number of holes, filling ratio, and small-scale impact on these behaviors [2]. These structures often interact with elastic foundations in engineering applications, and their mechanical behavior varies accordingly.

Classical beam theories (CTs) may be inadequate for analyzing nanoscale structures due to their inability to account for size-dependent effects [3]. Many higher-order elasticity theories have been proposed in the literature to overcome these deficiencies. One such theory is the Modified Couple Stress Theory (MCST) developed by Yang et al. [4]. This theory was introduced to capture these size effects by incorporating an intrinsic length scale parameter into the analysis. In recent years, many studies have been conducted to analyze the mechanical behavior of nanostructures using MCST [5] - [12].

The stability of beams on elastic foundations has been studied using various foundation models. The Winkler elastic foundation (WEF) model, widely used due to its simplicity, models the interaction between the foundation and the beam with springs [13], [14]. The Winkler-Pasternak elastic foundation (W-PEF) model improved the WEF model by including the shear interactions between the spring elements [15], [16]. There have been many studies investigating the mechanical behavior of nanostructures using elastic foundation models and MCST [17] - [21]. Togun and Bağdatlı [18] developed an MCST-based model to analyze the free vibration behavior of simply supported (S-S) nanobeams resting on a WEF. By employing Hamilton's principle and the multiple scale method, their study demonstrates that the incorporation of a

***Corresponding Author:** Uğur KAFKAS, ugur.kafkas@dpu.edu.tr

material length scale parameter effectively captures significant size effects—yielding higher fundamental frequencies than those predicted by classical Euler–Bernoulli theory—and that an increased non-dimensional Winkler foundation parameter enhances system stiffness. Akgöz ve Civalek [18] investigated the free vibration behavior of single-layered graphene sheets on a Pasternak-type elastic matrix using MCST and an analytical thin plate model. Their analytical results demonstrate that the material length scale parameter significantly affects the vibration frequencies—especially for smaller geometries and higher vibration modes—with its influence diminishing as the Winkler and shear modulus parameters increase. Şimşek [21] developed a non-classical beam model for the static and nonlinear vibration analysis of microbeams on a three-layered nonlinear elastic foundation by integrating MCST with Euler–Bernoulli beam theory and incorporating von-Kármán's geometric nonlinearity. The study reveals that the inclusion of a length scale parameter and nonlinear foundation stiffness coefficients significantly influences both the static deflection and the nonlinear frequency ratio, with the derived closed-form expressions being validated through extensive numerical comparisons.

Perforated nanobeams are nanostructures with modified stiffness properties created using various techniques and must be modeled appropriately [22]. Luschi and Pieri [23] proposed a local model for the micromechanical properties of microscale perforated beams. Although many researchers have studied either perforated macro/nano beams [24] - [35] or nanobeams on elastic foundations [36] - [44], the effects of hole patterns and elastic foundation interactions on nanobeam buckling behavior have not been sufficiently investigated. Abdelrahman et al. [36] modeled the buckling behavior of perforated nanobeams in a piezoelectric sandwich structure, considering elasticity and dimensional effects. Almitani et al. [37] performed the stability analysis of perforated nanorods, considering the surface energy effect. Abdelrahman and Eltaher [2] investigated the bending and buckling responses of perforated nanobeams, examining the effects of surface energy on different beam theories. Eltaher et al. [38] analytically investigated the static bending and buckling behavior of perforated nanobeams according to Euler-Bernoulli and Timoshenko theories, considering nonlocal effects. Kafkas et al. [22] proposed an analytical solution by considering non-local effects and deformable boundary conditions while investigating the buckling behavior of perforated nano/microbeams on an elastic foundation.

This study makes a novel contribution to the field of nanostructure mechanics by integrating MCST with FEM for analyzing the buckling behavior of perforated nanobeams on W-PEF. Unlike traditional analyses based solely on classical continuum theories, this study explicitly accounts for nanoscale size effects through the incorporation of an intrinsic length scale parameter. A comprehensive literature review indicates that no previous work has addressed the buckling behavior of perforated nanobeams on W-PEF using MCST, either analytically or numerically. These contributions not only extend the theoretical framework for understanding nanoscale buckling phenomena but also offer guidance for designing and optimizing advanced nanostructured materials.

2. MATERIAL AND METHODS

The geometrical configuration of a S-S perforated nanobeam loaded by an axial force P, defined by the presence of holes of dimensions L, b and h in the cross-sectional region, is shown in Figure 1.

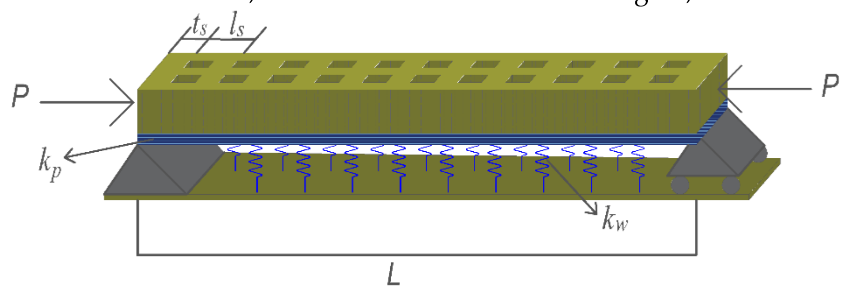

Figure 1. Perforated nanobeam resting on a W-PEF

To effectively analyze the mechanical response of perforated structures, it is essential to consider the periodic arrangement of the cut-out holes. Luschi and Pieri [23] presented analytical solutions for equivalent geometric and material properties of perforated beams. Let l_s and t_s denote the spatial period and period length, respectively, and the filling ratio α can be represented as follows [23]:

$$\alpha = \frac{t_s}{l_s}, \quad 0 < \alpha \leq 1 \tag{1}$$

The critical point to note here is that in the case of $\alpha = 1$, the nanobeam represents a fully filled solid beam, while $\alpha < 1$ refers to the case with holes [29]. N indicates the number of holes along the cross-section, the equivalent bending stiffness and shear stiffness of the perforated beam compared to the solid beam can be expressed as follows [23], [38] - [40]:

$$\frac{(EI)_p}{EI} = \frac{\alpha(N+1)(N^2+2N+\alpha^2)}{(1-\alpha^2+\alpha^3)N^3+3\alpha N^2+(3\alpha^2+2\alpha^3-3\alpha^4+\alpha^5)N+\alpha^3} \tag{2}$$

$$\frac{(GA)_p}{EA} = \frac{\alpha^3(N+1)}{2N} \tag{3}$$

where E and G represent the modulus of elasticity and shear, A and I represent the cross-sectional area and moment of inertia of the filled beam, respectively, and $A = bh$. The sub-index p represents the perforated nano-beam.

2.1. Modified Couple Stress Theory

MCST, first proposed by Yang et al. [4], accounts for the small size effects observed in micro- and nanoscale structures by incorporating a material length scale parameter into its equations. According to MCST, for a solid nano-beam resting on a W-PEF, the governing equation for the buckling problem can be represented as follows [41], [42]:

$$EI\frac{\partial^4 w}{\partial x^4} + GAl_m^2\frac{\partial^4 w}{\partial x^4} + P\frac{\partial^2 w}{\partial x^2} - k_p\frac{\partial^2 w}{\partial x^2} + k_w w = 0 \tag{4}$$

where EI and GA are the bending and shear stiffnesses of the solid beam, respectively, l_m is the material length scale parameter, k_w and k_p are the WEF and W-PEF parameters, respectively, and w is the transverse displacement. If the bending and shear stiffnesses of the perforated nano-beam given in Equations (2) and (3) are substituted in Equation (4), the governing equation can be shown as follows:

$$[(EI)_P + (GA)_P l_m^2]\frac{\partial^4 w}{\partial x^4} + [P - k_p]\frac{\partial^2 w}{\partial x^2} + k_w w = 0 \tag{5}$$

2.2. Finite Element Method

To examine the buckling behavior of a nanobeam resting on a W-PEF via the FEM and to determine the critical buckling loads by accounting for the size effect using the MCST, the nanobeam is discretized into more minor beam elements.

2.2.1 Finite element discretization process

The nanobeam is discretized into N^e finite elements, each consisting of two nodes with four degrees of freedom (DOF) per element—two translational (w_1, w_2) and two rotational (θ_1, θ_2) DOFs. The shape functions $\boldsymbol{\xi}$ are employed to interpolate the displacement field within each element based on nodal values. The governing differential equation, incorporating MCST effects, is formulated in its weak form to facilitate FEM implementation. The nodal displacement vector, $\mathbf{w}$, represents the displacements and rotations at both ends of the beam element and is shown as follows [43]:

$$\mathbf{w} = [w_1 \quad \theta_1 \quad w_2 \quad \theta_2] \tag{6}$$

where w_1 and θ_1 represent the transverse displacement and rotation at node 1 and w_2 and θ_2 represent the transverse displacement and rotation at node 2, respectively.

The shape functions can be given as follows [44]:

$$\boldsymbol{\xi} = \begin{bmatrix} \xi_1 \\ \xi_2 \\ \xi_3 \\ \xi_4 \end{bmatrix} \tag{7}$$

Both the displacement and rotation of the nanobeam at each nodal point can be represented by the shape functions as follows:

$$w = w_1\xi_1 + \theta_1\xi_2 + w_2\xi_3 + \theta_2\xi_4 \tag{8}$$

Given the length L_e of each beam segment, the elements of the shape function vector can be defined as follows [44]:

$$\boldsymbol{\xi} = \begin{bmatrix} \xi_1 \\ \xi_2 \\ \xi_3 \\ \xi_4 \end{bmatrix} = \begin{bmatrix} 1 - \dfrac{3x^2}{L_e^2} + \dfrac{2x^3}{L_e^3} \\ x - \dfrac{2x^2}{L_e} + \dfrac{x^3}{L_e^2} \\ \dfrac{3x^2}{L_e^2} - \dfrac{2x^3}{L_e^3} \\ -\dfrac{x^2}{L_e} + \dfrac{x^3}{L_e^2} \end{bmatrix} \tag{9}$$

According to the MCST with a small-scale effect, to obtain the weak form of the governing differential equation for buckling of a nanobeam on a W-PEF, shape functions can be chosen as weighting functions, and the differential equation can be formulated in weighted integral form. This requires multiplying the residual R by the weighting functions and integrating the result over the entire length of the nanobeam:

$$R = [(EI)_P + (GA)_P l_m^2]\frac{\partial^4 w}{\partial x^4} + [P - k_p]\frac{\partial^2 w}{\partial x^2} + k_w w \tag{10}$$

$$\int_0^L \left([(EI)_P + (GA)_P l_m^2]\boldsymbol{\xi}\frac{\partial^4 w}{\partial x^4} + [P - k_p]\boldsymbol{\xi}\frac{\partial^2 w}{\partial x^2} + k_w\boldsymbol{\xi}w \right) dx = 0 \tag{11}$$

Parts integrate equation (11), and the chain rule is used to obtain the general form:

$$\int_0^L \left([(EI)_P + (GA)_P l_m^2]\frac{d^2\boldsymbol{\xi}}{dx^2}\frac{d^2\boldsymbol{\xi}^T}{dx^2} + [P - k_p]\frac{d\boldsymbol{\xi}}{dx}\frac{d\boldsymbol{\xi}^T}{dx} + k_w\boldsymbol{\xi}\boldsymbol{\xi}^T \right) dx = 0 \tag{12}$$

2.2.2 Solution steps in the FEM approach

To determine the critical buckling load of the perforated nanobeam using FEM, the following solution procedure is applied:

1. Discretization: The nanobeam is divided into N^e elements, each modeled using two-node beam elements that incorporate transverse displacement and rotation.
2. Shape Function Definition: The displacement field is approximated using Hermite cubic shape functions, ensuring continuity in displacement and rotation.
3. Weak Formulation: The governing equation is rewritten in weighted residual form, where shape functions serve as weighting functions, allowing the formulation of the stiffness matrix K and load matrix B.
4. Stiffness and Load Matrix Computation: The global system matrices are assembled based on element contributions.
5. Eigenvalue Problem Solving: The characteristic equation $|K - \lambda B| = 0$ is solved to determine the critical buckling load, where $\lambda = P_{cr}/P$ represents the eigenvalue.

To derive the global system matrices; the stiffness, elastic foundation and axial load matrices of the nanobeam, the shape functions in Equation (9) are substituted in Equation (12), and integrals are performed term by term. The resulting matrices are defined below:

$$K_L = (EI)_P \int_0^{L_e} \begin{Bmatrix} \xi_1'' \\ \xi_2'' \\ \xi_3'' \\ \xi_4'' \end{Bmatrix} \{\xi_1'' \quad \xi_2'' \quad \xi_3'' \quad \xi_4''\} dx = \frac{(EI)_P}{L_e^3} \begin{bmatrix} 12 & 6L_e & -12 & 6L_e \\ 6L_e & 4L_e^2 & -6L_e & 2L_e^2 \\ -12 & -6L_e & 12 & -6L_e \\ 6L_e & 2L_e^2 & -6L_e & 4L_e^2 \end{bmatrix} \tag{13}$$

$$K_M = (GA)_P l_m^2 \int_0^{L_e} \begin{Bmatrix} \xi_1'' \\ \xi_2'' \\ \xi_3'' \\ \xi_4'' \end{Bmatrix} \{\xi_1'' \quad \xi_2'' \quad \xi_3'' \quad \xi_4''\} dx = \frac{(GA)_P l_m^2}{L_e^3} \begin{bmatrix} 12 & 6L_e & -12 & 6L_e \\ 6L_e & 4L_e^2 & -6L_e & 2L_e^2 \\ -12 & -6L_e & 12 & -6L_e \\ 6L_e & 2L_e^2 & -6L_e & 4L_e^2 \end{bmatrix} \tag{14}$$

$$K_W = k_W \int_0^{l_e} \begin{Bmatrix} \xi_1 \\ \xi_2 \\ \xi_3 \\ \xi_4 \end{Bmatrix} \{\xi_1 \quad \xi_2 \quad \xi_3 \quad \xi_4\} dx = \frac{k_w}{420} \begin{bmatrix} 156L_e & 22L_e & 54L_e & -13L_e^2 \\ 22L_e^2 & 4L_e^3 & 13L_e^2 & -3L_e^3 \\ 54L_e & 13L_e^2 & 156L_e & -22L_e^2 \\ -13L_e^2 & -3L_e^3 & -22L_e^2 & 4L_e^3 \end{bmatrix} \tag{15}$$

$$K_P = k_p \int_0^{L_e} \begin{Bmatrix} \xi_1' \\ \xi_2' \\ \xi_3' \\ \xi_4' \end{Bmatrix} \{\xi_1' \quad \xi_2' \quad \xi_3' \quad \xi_4'\} dx = \frac{k_p}{30L_e} \begin{bmatrix} 36 & 3L_e & -36 & 3L_e \\ 3L_e & 4L_e^2 & -3L_e & -L_e^2 \\ -36 & -3L_e & 36 & -3L_e \\ 3L_e & -L_e^2 & -3L_e & 4L_e^2 \end{bmatrix} \tag{16}$$

$$B_A = P \int_0^{l_e} \begin{Bmatrix} \xi_1' \\ \xi_2' \\ \xi_3' \\ \xi_4' \end{Bmatrix} \{\xi_1' \quad \xi_2' \quad \xi_3' \quad \xi_4'\} dx = \frac{P}{420} \begin{bmatrix} 156L_e & 22L_e & 54L_e & -13L_e^2 \\ 22L_e^2 & 4L_e^3 & 13L_e^2 & -3L_e^3 \\ 54L_e & 13L_e^2 & 156L_e & -22L_e^2 \\ -13L_e^2 & -3L_e^3 & -22L_e^2 & 4L_e^3 \end{bmatrix} \tag{17}$$

In these equations, K_L is the matrix derived from the CT (local), K_M is the matrix related to MCST, which also takes into account the effect of small size by means of the material length scale parameter. If the K_M matrix is neglected, the finite element solution reduces to the Euler-Bernoulli beam theory based on classical mechanics. The K_W and K_P matrices are due to the WEF parameter and the Pasternak shear layer effect, respectively, while the B_A matrix is the matrix due to the axial load. From the K_W and K_P matrices, if the K_P matrix is neglected, buckling analysis to MCST can be performed for the nano-beam resting on a WEF, while if both K_W and K_P are neglected, the buckling behavior of the nano-beam not resting on an elastic foundation is analyzed.

The buckling loads of a nanobeam resting on the W-PEF can be calculated according to MCST using the total stiffness and load matrices as follows [45]:

$$|K - \lambda B| = 0 \tag{18}$$

where λ eigenvalue represents the ratio of the critical buckling load (P_{cr}) to the applied axial load (P), K is the sum of the stiffness matrices, and B is the sum of the matrices resulting from the axial load and is shown as:

$$\lambda = \frac{P_{cr}}{P} \tag{19}$$
$$[K] = [K_L] + [K_M] + [K_W] + [K_P] \tag{20}$$
$$[B] = [B_A] \tag{21}$$

3. RESULTS AND DISCUSSION

This chapter examines the critical buckling loads of nanobeams resting on a W-PEF using numerical results based on the MCST, considering the effects of size and elastic foundation. The study provides a FEM-based solution, and analyses are conducted to validate the results and to explore the influence of various parameters on the buckling behavior of nanobeams. For these analyses, as well as the presentation of figures and tables, the following dimensionless quantities are employed:

$$K^w = \frac{k_w L^4}{EI} \tag{22}$$
$$K^p = \frac{k_p L^2}{EI} \tag{23}$$

A comparison study to verify the accuracy of the FEM model is presented in this section. The analytical solution of critical buckling loads according to MCST for a S-S solid nanobeam resting on the W-PEF is given by Mercan et al. [41] as follows:

$$\overline{P(n)} = (EI + GAl_m^2)\frac{n^2\pi^2}{L^2} + \frac{k_w L^2}{n^2\pi^2} + k_p \tag{24}$$

where n is the mode number of the buckling.

By substituting the equivalent bending stiffness and shear stiffness of the perforated beams, derived from Equations (2) and (3), into Equation (24), the critical buckling loads according to the MCST for a S-S perforated nanobeam resting on a W-PEF can be analytically determined. In Equation (24), the smallest load ($n = 1$) is called the critical buckling load [46] and can be calculated as follows:

$$P_{cr} = [(EI)_P + (GA)_P l_m^2]\frac{\pi^2}{L^2} + \frac{k_w L^2}{\pi^2} + k_p \tag{25}$$

The analytically calculated critical buckling loads, along with the results obtained from the FEM model for varying element numbers, are presented in Table 1. The geometrical and material properties of the perforated nanobeam are given as follows in Table 1 and in the rest of the study unless otherwise stated: $E = 1$ TPa, $h = 2$ nm, $b = 4$ nm, $K^w = 100$, $K^p = 5$, $N = 5$, $\alpha = 0.5$, and $l_m = 0.5$. Comparisons are made for different values of L and N^e.

Table 1. Comparison of critical buckling loads (P_{cr}) obtained from Equation (25) and FEM for different values of L and N^e

L (nm)	P_{cr} (nN)					
	Eq. 25	FEM				
		$N^e = 10$	$N^e = 15$	$N^e = 20$	$N^e = 25$	$N^e = 30$
10	602.3807	602.3834	602.3812	602.3809	602.3808	602.3807
20	150.5952	150.5958	150.5953	150.5952	150.5952	150.5952
30	66.9312	66.9315	66.9312	66.9312	66.9312	66.9312
40	37.6488	37.6490	37.6488	37.6488	37.6488	37.6488
50	24.0952	24.0953	24.0952	24.0952	24.0952	24.0952

From Table 1, the analytical solution given in Equation (25) closely matches the solution provided by the FEM. For all other L lengths except $L = 10$ nm, the $N^e = 20$ case gives exact results up to four digits after the integer. In the case of $L = 10$, the exact result is obtained at $N^e = 30$. In the analyses performed throughout the study, $N^e = 30$ was chosen considering this situation, and all analyses were performed according to this value.

Figure 2 compares the critical buckling loads of a perforated nanobeam resting on a W-PEF as predicted by CT and MCST. The numerical values employed in this figure are consistent with those listed in Table 1. Two different length-scale parameters are selected for MCST: $l_m = 1$ nm. and $l_m = 2$ nm.

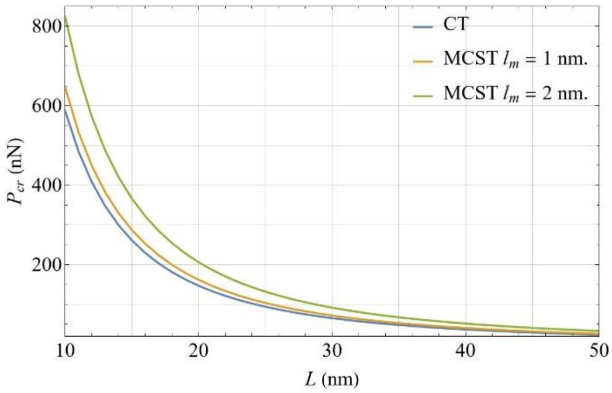

Figure 2. Comparison of the critical buckling loads for CT and MCST

In applying the MCST, the length scale parameter is typically determined by comparing experimentally measured size-dependent mechanical responses—such as bending stiffness, natural frequencies, or related behaviors at micro/nano scales—with theoretical predictions from MCST. Yang et al. [4] have outlined methodological approaches whereby experimental micro-scale data are modeled under the MCST framework to obtain the corresponding material length scale. Similarly, Park and Gao [47] employed variational methods to derive closed-form solutions, thereby highlighting the importance of calibrating l_m based on the bending and vibration responses of micro-beams. Their findings indicate that l_m is closely tied to the microstructural characteristics of the material, such as grain size, crystal structure, or atomic-level regularity. Due to the scarcity of comprehensive nano-scale experimental data—often stemming from the high costs and complexities of conducting such experiments—the range $0 < l_m/h \leq 1$ is frequently adopted in the literature [26], [41], [48]. This practical choice captures a broad spectrum of microstructural effects without requiring exhaustive experimental calibration for every specific material. As seen in Figure 2, MCST yields consistently higher critical buckling loads than the CT, demonstrating the enhanced stiffness arising from material microstructure effects.

Figure 3 demonstrates the effects of the elastic foundation on the critical buckling load. The analysis uses previously mentioned material and geometrical properties with $L = 30$ nm. The figure presents critical buckling loads for various values of K^w and K^p.

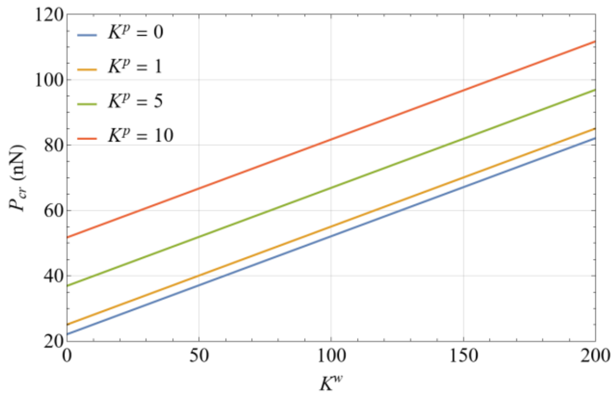

Figure 3. The critical buckling loads for different values of dimensionless elastic foundation parameters

The results show that critical buckling load values increase continuously as the dimensionless WEF parameter (K^w) increases, indicating more vital interaction between the nanobeam and foundation, thereby growing stiffness. The WEF model simulates foundation resistance using a spring analogy - as this resistance increases, the beam's buckling resistance also increases. This linear relationship shows that K^w's effect on critical buckling load is consistent across all values, meaning the beam's buckling stability is directly proportional to foundation stiffness. Figure 3 displays four curves representing different dimensionless Pasternak parameter (K^p) values (0, 1, 5, 10). The critical buckling load increases with K^p, similar to K^w. The Pasternak parameter enhances foundation stiffness by incorporating shear deformations, making the nanobeam more resistant to buckling. Even when $K^p = 0$, the buckling load increases with K^w, and this trend becomes more pronounced when K^p is included in the analysis. This demonstrates that the beam achieves greater stability when the foundation is modeled using both the spring analogy (Winkler) and shear effects (Pasternak). Each curve in Figure 3 corresponds to a specific K^p value, showing P_{cr} increasing with K^w. Higher K^p values yield greater P_{cr} values for equivalent K^w values. Notably, K^p has a significantly greater effect on the nanobeam's P_{cr} value than K^w. For instance, when $K^p = 0$, increasing K^w from 0 to 100 results in approximately 135% increase in P_{cr}. Similarly, when $K^w = 0$, increasing K^p from 0 to 10 produces a comparable percentage increase in P_{cr}, demonstrating how shear effects substantially strengthen the beam's buckling capacity. To further elucidate the combined effects of the K^w and K^p foundation parameters on the critical buckling load, Figure 4 has been added. This figure offers a comprehensive visualization of the interaction between K^w, K^p, and P_{cr}, clearly depicting how simultaneous variations in both foundation parameters influence buckling behavior.

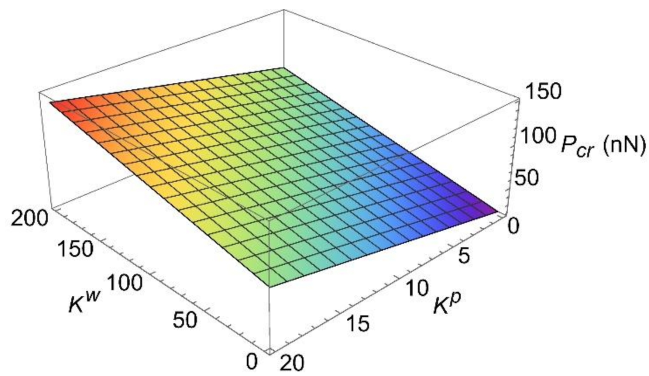

Figure 4. Variation of the critical buckling loads depending on K^w and K^p

Figures 5 and 6 illustrate how P_{cr} varies with the filling ratio and hole number while also revealing the effect of MCST's length scale parameter. The analysis uses $K^w = 100$ and $K^p = 5$, with $l_m = 0.1$ in Figure 5 and $l_m = 2$ in Figure 6, allowing examination of cases where MCST's effect is minimal and maximal, respectively.

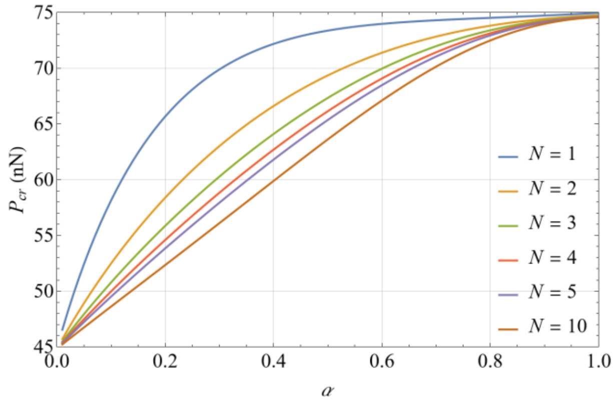

Figure 5. Variation of the critical buckling loads depending on α and N ($l_m = 0.1$)

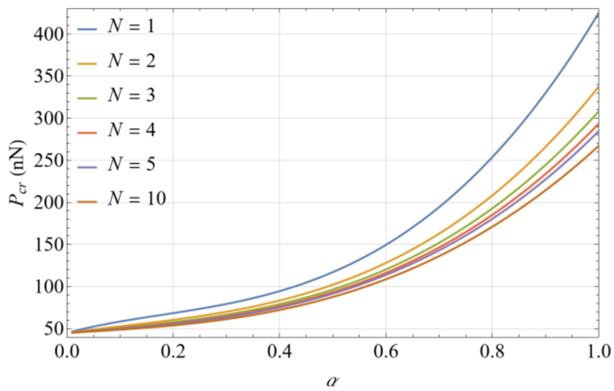

Figure 6. Variation of the critical buckling loads depending on α and N ($l_m = 2$)

Figures 5 and 6 illustrate the relationship between the critical buckling load, the filling ratio, and the number of holes in perforated nanobeams. The results indicate that P_{cr} increases significantly as α approaches 1, meaning that a fully filled beam exhibits higher buckling resistance. For a given α, an increase in N leads to a decrease in P_{cr}, as more perforations reduce the overall stiffness, thereby diminishing the buckling resistance. When $N = 1$, the nanobeam retains the highest P_{cr}, confirming that fewer perforations contribute to greater structural rigidity. Conversely, when $N = 10$, the increased number of perforations weakens the structure, leading to lower P_{cr} values. A key observation is the influence of the internal length scale parameter on buckling resistance. Comparing different cases ($l_m = 0.1$ versus $l_m = 2$) reveals that a larger l_m significantly increases P_{cr}, demonstrating that MCST accounts for microscale effects that enhance the beam's stiffness.

This effect is particularly evident in Figures 5 and 6, where the $N = 1$ curve consistently exhibits the highest P_{cr} values. The difference between Figures 5 and 6 is attributed solely to the variation in l_m. This discrepancy can be explained by examining the role of shear stiffness, which is influenced by l_m. As seen in the governing equation, the term $(GA)_P l_m^2$ contributes directly to P_{cr}. When l_m is small, $(GA)_P$ has a limited effect, leading to a concave downward trend in Figure 5. However, when l_m is large, the influence of $(GA)_P$ becomes more pronounced, smoothing out the increase in P_{cr} as α increases, resulting in a convex upward trend in Figure 6. This finding reveals the role of micro-scale shear effects in determining the buckling response of perforated nanobeams. Furthermore, the relationship between α and N indicates that although Pcr generally increases with α, this effect diminishes as N increases. In other words, when a nanobeam has a high number of perforations, increasing the filling ratio has a limited impact on its buckling strength. This suggests that the structural weakening effect caused by perforations depends not only on α but also on N and lm, demonstrating the necessity of incorporating non-classical continuum theories for accurate stability predictions in nanoscale beams.

Figure 7 provides a detailed examination of MCST's length scale parameter effect, showing P_{cr} variation as a function of l_m and N.

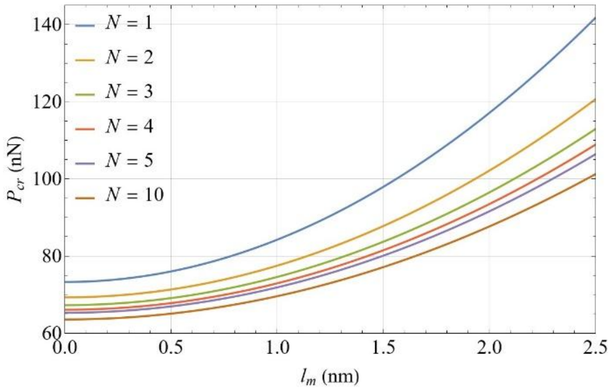

Figure 7. Variation of the critical buckling loads depending on l_m and N

The results clearly demonstrate increasing P_{cr} values with higher l_m values, indicating how the MCST's l_m parameter contributes to beam stiffness at nanoscale dimensions. This shows that size effects, significant at nano dimensions, enhance stiffness and buckling resistance. P_{cr} decreases with increasing N, and this effect becomes more pronounced at higher l_m values. The P_{cr} difference between $N = 1$ and $N = 10$ is approximately 13.25% at $l_m = 0.02$ nm, increasing to 28.60% at $l_m = 2.5$ nm. However, higher l_m values mitigate the holes' weakening effect on the beam. For instance, the P_{cr} value for $N = 1$ and $l_m = 0$ (CT) is lower than for $N = 10$ and $l_m = 1.3$ nm. This demonstrates how l_m's positive contribution to nanobeam stability can match or exceed P_{cr} values even with more holes. These findings indicate that the internal length parameter counterbalances hole-induced structural weakening by increasing stiffness in nano-sized structures. Consequently, with higher l_m parameter values, critical buckling load can remain high despite increased hole numbers.

Figure 8 analyzes the relationship between critical buckling loads and nanobeam length for varying numbers of holes.

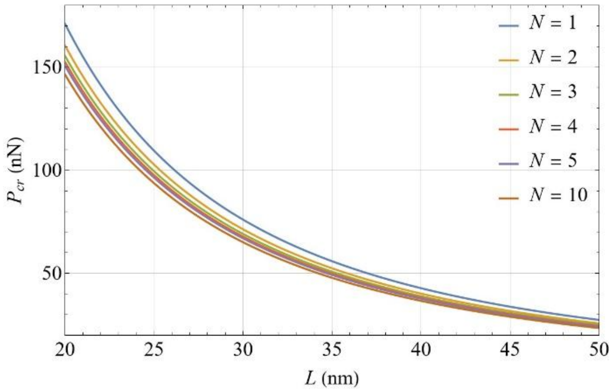

Figure 8. Variation of the critical buckling loads depending on L and N

The analysis demonstrates that critical buckling load decreases as beam length increases, confirming that longer beams have lower buckling resistance. This trend is consistent across all hole configurations. Beams with fewer holes maintain higher critical buckling load values even as length increases, indicating that structural stiffness decreases significantly with both increased hole numbers and the nanobeam length. Comparing configurations from $N = 1$ to $N = 10$ reveals that a higher number of holes substantially reduces critical buckling load. This reduction occurs because holes diminish the beam's overall structural stiffness, lowering its buckling resistance. The $N = 10$ configuration yields the lowest critical buckling load values, demonstrating the negative impact of multiple holes on structural stability.

Figures 9 through 12 examine elastic foundation effects on critical buckling load. Figures 9 and 11 plot results for $K^p = 5$ with varying K^w values, while Figures 10 and 12 show results for $K^w = 100$ with varying K^p values. Figures 9 and 10 analyze effects relative to the number of holes, while Figures 11 and 12 examine effects relative to the filling ratio.

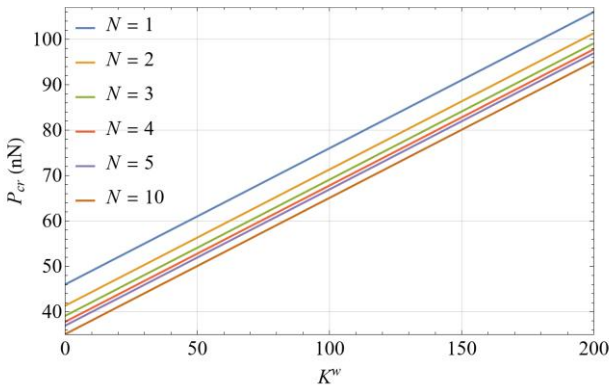

Figure 9. Variation of the critical buckling loads depending on K^w and N ($K^p = 5$)

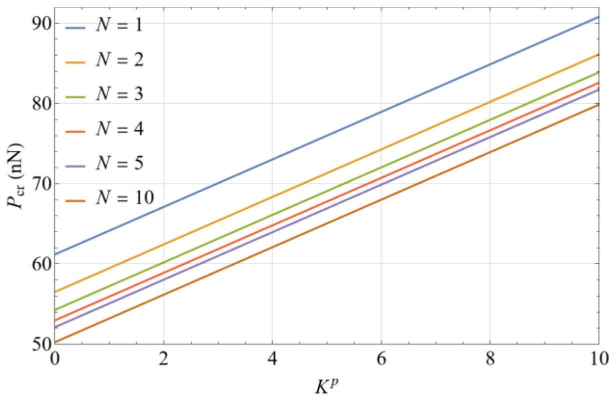

Figure 10. Variation of the critical buckling loads depending on K^p and N ($K^w = 100$)

Figure 9 demonstrates that critical buckling load increases with higher WEF parameter values. However, increasing the number of holes (from $N = 1$ to $N = 10$) significantly reduces critical buckling load. The holes weaken structural stiffness, diminishing the foundation stiffness's positive effect on critical buckling load. Beams with fewer holes ($N = 1$) exhibit higher buckling loads, indicating that foundation stiffness more effectively enhances structural stability in these cases. Similarly, Figure 10 shows that the critical buckling load increases with higher Pasternak foundation parameter values. The Pasternak foundation model's incorporation of shear effects enhances beam stiffness, improving buckling resistance. While critical buckling load still decreases with increased hole numbers, higher K^p values partially compensate for hole-induced weakening through increased foundation shear stiffness. Nevertheless, configurations with more holes ($N = 10$) maintain lower critical buckling loads, indicating that hole-induced weakening dominates despite increased foundation stiffness. Both figures demonstrate that critical buckling load increases with higher K^w and K^p parameters due to enhanced elastic foundation support, though increased hole numbers consistently reduce critical buckling load.

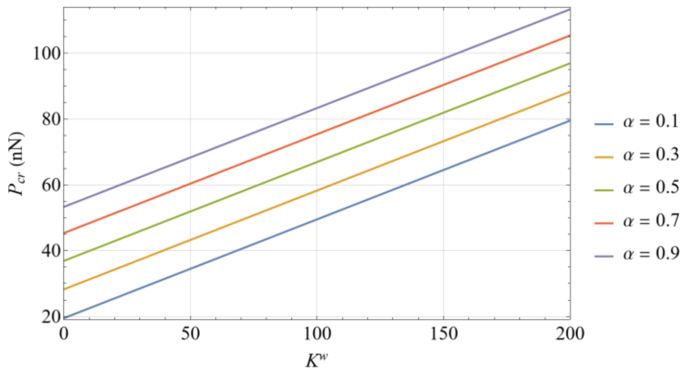

Figure 11. Variation of the critical buckling loads depending on K^w and α ($K^p = 5$)

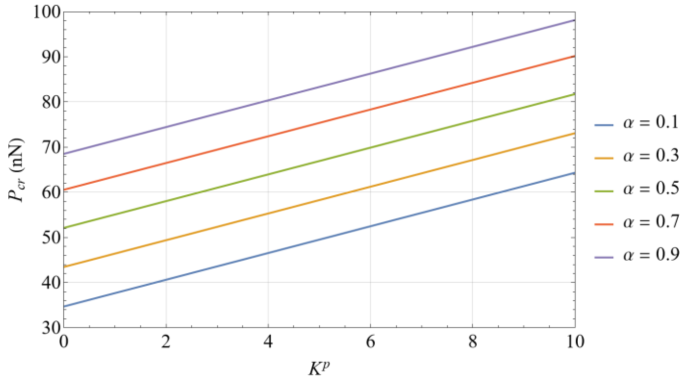

Figure 12. Variation of the critical buckling loads depending on K^p and α ($K^w = 100$)

Figures 11 and 12 reveal that critical buckling load increases significantly with higher filling ratios, indicating enhanced structural stiffness and buckling resistance. Both foundation parameters (K^w and K^p) positively affect P_{cr}. Figure 11 clearly shows P_{cr} increasing with K^w, demonstrating enhanced buckling resistance as foundation support strengthens. Additionally, P_{cr} increases linearly with the filling ratio (as α increases from 0.1 to 0.9). Figure 12 shows that similar P_{cr} increases with higher K^p values. P_{cr} consistently increases with α for each K^p value, demonstrating that higher filling ratios combined with foundation shear stiffness provide enhanced buckling resistance.

4. CONCLUSIONS

This study contributes to the field of nanostructure mechanics by investigating the buckling behavior of perforated nanobeams resting on W-PEF using MCST and FEM. This analysis significantly extends previous work on nanoscale buckling by incorporating size effects through MCST—an approach not previously applied to perforated nanobeams on W-PEF. The results demonstrate several key findings that advance the understanding of nanoscale mechanical behavior:

- Both Winkler and Pasternak foundation parameters substantially increase critical buckling loads, with the Pasternak foundation demonstrating superior influence due to its incorporation of shear effects. This finding aligns with previous research [16], [18] - [20], on beam–foundation interaction but extends the literature by examining perforated nanobeams at the nanoscale.
- The inclusion of the internal length scale parameter increases the predicted buckling capacity, emphasizing the need to account for size-dependent microstructural effects. These results support previous MCST-based studies on nano-beams without holes [41] - [43], but additionally demonstrate the interaction between holes and microstructural stiffness.
- Higher fill ratios are associated with increased buckling resistance, while additional holes reduce structural stability. Unlike macro-scale studies that treat holes as simple mass

reduction, this analysis also reveals the interactions between holes, size effects and foundation properties at the nanoscale.
- Beam length exhibits an inverse relationship with buckling resistance, particularly pronounced in highly perforated configurations, indicating a heightened sensitivity to geometric parameters at the nanoscale.

These findings provide practical guidance for nanostructured material design, particularly for applications requiring optimized buckling resistance. Future research directions should include:
- Investigating temperature effects on perforated nanobeam stability, particularly for applications in extreme thermal environments.
- Exploring different nanomaterials (e.g., graphene, carbon nanotubes) with their respective size-dependent properties.
- Examining dynamic loading conditions and vibration response.
- Incorporating multi-physics coupling effects (electro-mechanical, thermo-mechanical) relevant to next-generation nano-devices.

The methodology developed in this study provides a framework for future investigations into complex nanostructure behavior where classical theories prove inadequate.

Declaration of Ethical Standards

The author(s) declare that they have carried out this completely original study by adhering to all ethical rules including authorship, citation and data reporting.

Credit Authorship Contribution Statement

Uğur Kafkas conceived and designed the study, analyzed the data and wrote the manuscript.

Declaration of Competing Interest

The author(s) declare that they have no known competing financial interests or personal relationships that could have appeared to influence the work reported in this paper.

Funding / Acknowledgements

The author(s) received no financial support for the research.

Data Availability

This study does not contain usable data.

REFERENCES

[1] M. A. Eltaher, A. Khairy, A. M. Sadoun, and F.-A. Omar, "Static and buckling analysis of functionally graded Timoshenko nanobeams," *Appl Math Comput*, vol. 229, pp. 283–295, Feb. 2014, doi: 10.1016/j.amc.2013.12.072.

[2] A. A. Abdelrahman and M. A. Eltaher, "On bending and buckling responses of perforated nanobeams including surface energy for different beams theories," *Eng Comput*, vol. 38, no. 3, pp. 2385–2411, Jun. 2022, doi: 10.1007/s00366-020-01211-8.

[3] M. Ö. Yaylı, "Stability analysis of a rotationally restrained microbar embedded in an elastic matrix using strain gradient elasticity," *Curved and Layered Structures*, vol. 6, no. 1, pp. 1–10, Jan. 2019, doi: 10.1515/cls-2019-0001.

[4] F. Yang, A. C. M. Chong, D. C. C. Lam, and P. Tong, "Couple stress based strain gradient theory for elasticity," *Int J Solids Struct*, vol. 39, no. 10, pp. 2731–2743, May 2002, doi: 10.1016/S0020-7683(02)00152-X.

[5] M. Ö. Yaylı, "Torsional vibrations of restrained nanotubes using modified couple stress theory," *Microsystem Technologies*, vol. 24, no. 8, pp. 3425–3435, Aug. 2018, doi: 10.1007/s00542-018-3735-3.

[6] S. K. Park and X.-L. Gao, "Bernoulli–Euler beam model based on a modified couple stress theory," *Journal of Micromechanics and Microengineering*, vol. 16, no. 11, pp. 2355–2359, Nov. 2006, doi: 10.1088/0960-1317/16/11/015.

[7] S. C. Polat and S. M. Bağdatlı, "Investigation of stepped microbeam vibration motions according to modified couple stress theory," *Zeitschrift für Naturforschung A*, vol. 78, no. 5, pp. 379–393, May 2023, doi: 10.1515/zna-2022-0286.

[8] B. Uzun and M. Ö. Yaylı, "Porosity dependent torsional vibrations of restrained FG nanotubes using modified couple stress theory," *Mater Today Commun*, vol. 32, p. 103969, Aug. 2022, doi: 10.1016/j.mtcomm.2022.103969.

[9] B. Uzun and M. Ö. Yaylı, "A Finite Element Solution for Bending Analysis of a Nanoframe using Modified Couple Stress Theory," *International Journal of Engineering and Applied Sciences*, vol. 14, no. 1, pp. 1–14, Sep. 2022, doi: 10.24107/ijeas.1064690.

[10] B. Uzun and M. Ö. Yaylı, "A Unified Technique for Stability Analysis of an Embedded FG Porous Nano/Microbeam Via Modified Couple Stress Theory," *Nano*, Jul. 2024, doi: 10.1142/S1793292024500723.

[11] B. Akgöz and Ö. Civalek, "Strain gradient elasticity and modified couple stress models for buckling analysis of axially loaded micro-scaled beams," *Int J Eng Sci*, vol. 49, no. 11, pp. 1268–1280, Nov. 2011, doi: 10.1016/j.ijengsci.2010.12.009.

[12] B. Uzun, U. Kafkas, and M. Ö. Yaylı, "Free vibration analysis of nanotube based sensors including rotary inertia based on the Rayleigh beam and modified couple stress theories," *Microsystem Technologies*, vol. 27, no. 5, pp. 1913–1923, May 2021, doi: 10.1007/s00542-020-04961-z.

[13] S. C. Pradhan and G. K. Reddy, "Buckling analysis of single walled carbon nanotube on Winkler foundation using nonlocal elasticity theory and DTM," *Comput Mater Sci*, vol. 50, no. 3, pp. 1052–1056, Jan. 2011, doi: 10.1016/J.COMMATSCI.2010.11.001.

[14] B. Uzun, Ö. Civalek, and M. Ö. Yaylı, "Vibration of FG nano-sized beams embedded in Winkler elastic foundation and with various boundary conditions," *Mechanics Based Design of Structures and Machines*, vol. 51, no. 1, pp. 481–500, Jan. 2023, doi: 10.1080/15397734.2020.1846560.

[15] N. Togun and S. Bağdatlı, "Nonlinear Vibration of a Nanobeam on a Pasternak Elastic Foundation Based on Non-Local Euler-Bernoulli Beam Theory," *Mathematical and Computational Applications*, vol. 21, no. 1, p. 3, Mar. 2016, doi: 10.3390/mca21010003.

[16] B. Uzun and M. Ö. Yaylı, "Porosity and Deformable Boundary Effects on the Dynamic of Nonlocal Sigmoid and Power-Law FG Nanobeams Embedded in the Winkler–Pasternak Medium," *Journal of Vibration Engineering & Technologies*, vol. 12, no. 3, pp. 3193–3212, Mar. 2024, doi: 10.1007/s42417-023-01039-8.

[17] W.-T. Park, S.-C. Han, W.-Y. Jung, and W.-H. Lee, "Dynamic instability analysis for S-FGM plates embedded in Pasternak elastic medium using the modified couple stress theory," *Steel and Composite Structures*, vol. 22, no. 6, pp. 1239–1259, Dec. 2016, doi: 10.12989/scs.2016.22.6.1239.

[18] N. Togun and S. M. Bağdatli, "The vibration of nanobeam resting on elastic foundation using modified couple stress theory," *Tehnički glasnik*, vol. 12, no. 4, pp. 221–225, Dec. 2018, doi: 10.31803/tg-20180214212115.

[19] B. Akgöz and Ö. Civalek, "Free vibration analysis for single-layered graphene sheets in an elastic matrix via modified couple stress theory," *Mater Des*, vol. 42, pp. 164–171, Dec. 2012, doi: 10.1016/j.matdes.2012.06.002.

[20] B. Akgöz and Ö. Civalek, "Modeling and analysis of micro-sized plates resting on elastic medium using the modified couple stress theory," *Meccanica*, vol. 48, no. 4, pp. 863–873, May 2013, doi: 10.1007/s11012-012-9639-x.

[21] M. Şimşek, "Nonlinear static and free vibration analysis of microbeams based on the nonlinear elastic foundation using modified couple stress theory and He's variational method," *Compos Struct*, vol. 112, pp. 264–272, Jun. 2014, doi: 10.1016/j.compstruct.2014.02.010.

[22] U. Kafkas, Y. Ünal, M. Ö. Yaylı, and B. Uzun, "Buckling analysis of perforated nano/microbeams with deformable boundary conditions via nonlocal strain gradient elasticity," *Adv Nano Res*, vol. 15, no. 4, pp. 339–353, 2023, doi: 10.12989/anr.2023.15.4.339.

[23] L. Luschi and F. Pieri, "An analytical model for the determination of resonance frequencies of perforated beams," *Journal of Micromechanics and Microengineering*, vol. 24, no. 5, p. 055004, May 2014, doi: 10.1088/0960-1317/24/5/055004.

[24] U. Kafkas, "On the free vibration of a perforated Rayleigh beam with deformable ends," *Engineering Science and Technology, an International Journal*, vol. 56, p. 101787, Aug. 2024, doi: 10.1016/J.JESTCH.2024.101787.

[25] A. A. Abdelrahman, M. A. Eltaher, A. M. Kabeel, A. M. Abdraboh, and A. A. Hendi, "Free and forced analysis of perforated beams," *Steel and Composite Structures*, vol. 31, no. 5, p. 489, 2019.

[26] B. Uzun and M. Ö. Yaylı, "Bending Analysis of A Perforated Microbeam With Laplace Transform," *Konya Journal of Engineering Sciences*, vol. 11, pp. 23–31, Dec. 2023, doi: 10.36306/konjes.1384835.

[27] A. Assie, Ş. D. Akbaş, A. H. Bashiri, A. A. Abdelrahman, and M. A. Eltaher, "Vibration response of perforated thick beam under moving load," *The European Physical Journal Plus*, vol. 136, no. 3, p. 283, Mar. 2021, doi: 10.1140/epjp/s13360-021-01224-2.

[28] M. A. Eltaher, R. A. Shanab, and N. A. Mohamed, "Analytical solution of free vibration of viscoelastic perforated nanobeam," *Archive of Applied Mechanics*, vol. 93, no. 1, pp. 221–243, Jan. 2023, doi: 10.1007/s00419-022-02184-4.

[29] U. Kafkas, B. Uzun, M. Ö. Yaylı, and G. Güçlü, "Thermal vibration of perforated nanobeams with deformable boundary conditions via nonlocal strain gradient theory," *Zeitschrift für Naturforschung A*, vol. 0, no. 0, Jun. 2023, doi: 10.1515/zna-2023-0088.

[30] Ö. Civalek, B. Uzun, and M. Ö. Yaylı, "Size-dependent nonlinear stability response of perforated nano/microbeams via Fourier series," *Archive of Applied Mechanics*, vol. 93, no. 12, pp. 4425–4443, Dec. 2023, doi: 10.1007/s00419-023-02501-5.

[31] B. Uzun, Ö. Civalek, and M. Ö. Yaylı, "Critical buckling loads of embedded perforated microbeams with arbitrary boundary conditions via an efficient solution method," *Zeitschrift für Naturforschung A*, vol. 78, no. 2, pp. 195–207, Feb. 2023, doi: 10.1515/zna-2022-0230.

[32] T. Küpeli, Y. H. Çavuş, B. Uzun, and M. Ö. Yaylı, "Free Vibration Response of a Steel Liquid Storage Tank with Porous and Perforated Columns via an Exact Continuum Method," *Gazi University Journal of Science*, vol. 36, no. 2, pp. 555–571, Jun. 2023, doi: 10.35378/gujs.1047479.

[33] M. A. Koç, M. Eroğlu, and İ. Esen, "Dynamic analysis of high-speed train moving on perforated Timoshenko and Euler–Bernoulli beams," *International Journal of Mechanics and Materials in Design*, vol. 18, no. 4, pp. 893–917, Dec. 2022, doi: 10.1007/s10999-022-09610-z.

[34] A. A. Abdelrahman, I. Esen, C. Özarpa, and M. A. Eltaher, "Dynamics of perforated nanobeams subject to moving mass using the nonlocal strain gradient theory," *Appl Math Model*, vol. 96, pp. 215–235, Aug. 2021, doi: 10.1016/j.apm.2021.03.008.

[35] A. A. Abdelrahman, I. Esen, C. Özarpa, R. Shaltout, M. A. Eltaher, and A. E. Assie, "Dynamics of perforated higher order nanobeams subject to moving load using the nonlocal strain gradient theory," *Smart Struct Syst*, vol. 28, no. 4, pp. 515–53, Oct. 2021, doi: 10.12989/sss.2021.28.4.515.

[36] A. A. Abdelrahman, H. E. Abdel-Mottaleb, A. Aljabri, E. R. I. Mahmoud, and M. A. Eltaher, "Modeling of size dependent buckling behavior of piezoelectric sandwich perforated nanobeams

rested on elastic foundation with flexoelectricity," *Mechanics Based Design of Structures and Machines*, pp. 1–27, Jun. 2024, doi: 10.1080/15397734.2024.2365918.

[37] K. H. Almitani, A. A. Abdelrahman, and M. A. Eltaher, "Stability of perforated nanobeams incorporating surface energy effects," *Steel and Composite Structures, An International Journal*, vol. 35, no. 4, pp. 555–566, 2020.

[38] M. A. Eltaher, A. M. Kabeel, K. H. Almitani, and A. M. Abdraboh, "Static bending and buckling of perforated nonlocal size-dependent nanobeams," *Microsystem Technologies*, vol. 24, no. 12, pp. 4881–4893, Dec. 2018, doi: 10.1007/s00542-018-3905-3.

[39] I. Esen, A. A. Abdelrahman, and M. A. Eltaher, "Dynamics analysis of timoshenko perforated microbeams under moving loads," *Eng Comput*, vol. 38, no. 3, pp. 2413–2429, Jun. 2022, doi: 10.1007/s00366-020-01212-7.

[40] M. A. Eltaher, A. M. Abdraboh, and K. H. Almitani, "Resonance frequencies of size dependent perforated nonlocal nanobeam," *Microsystem Technologies*, vol. 24, no. 9, pp. 3925–3937, Sep. 2018, doi: 10.1007/s00542-018-3910-6.

[41] K. Mercan, H. M. Numanoglu, B. Akgöz, C. Demir, and Ö. Civalek, "Higher-order continuum theories for buckling response of silicon carbide nanowires (SiCNWs) on elastic matrix," *Archive of Applied Mechanics*, vol. 87, no. 11, pp. 1797–1814, Nov. 2017, doi: 10.1007/s00419-017-1288-z.

[42] Ö. Civalek, H. Numanoğlu, and K. Mercan, "Finite Element Model and Size Dependent Stability Analysis of Boron Nitride and Silicon Carbide Nanowires/Nanotubes," *Scientia Iranica*, vol. 0, no. 0, pp. 0–0, Apr. 2019, doi: 10.24200/sci.2019.52517.2754.

[43] Ç. Demir and Ö. Civalek, "A new nonlocal FEM via Hermitian cubic shape functions for thermal vibration of nano beams surrounded by an elastic matrix," *Compos Struct*, vol. 168, pp. 872–884, May 2017, doi: 10.1016/J.COMPSTRUCT.2017.02.091.

[44] J. N. Reddy, *Energy Principles and Variational Methods in Applied Mechanics* , 2. New York: John Wiley and Sons, 2002.

[45] J. K. Phadikar and S. C. Pradhan, "Variational formulation and finite element analysis for nonlocal elastic nanobeams and nanoplates," *Comput Mater Sci*, vol. 49, no. 3, pp. 492–499, Sep. 2010, doi: 10.1016/j.commatsci.2010.05.040.

[46] M. Şimşek, "Some closed-form solutions for static, buckling, free and forced vibration of functionally graded (FG) nanobeams using nonlocal strain gradient theory," *Compos Struct*, vol. 224, p. 111041, Sep. 2019, doi: 10.1016/j.compstruct.2019.111041.

[47] S. K. Park and X.-L. Gao, "Variational formulation of a modified couple stress theory and its application to a simple shear problem", *Zeitschrift für angewandte Mathematik und Physik*, 59:904–917, 2008, doi: 10.1007/s00033-006-6073-8.

[48] J. N. Reddy, "Microstructure-dependent couple stress theories of functionally graded beams", *J Mech Phys Solids*, 59:2382–2399, 2011, doi: 10.1016/j.jmps.2011.06.008.